PCCP

PAPER

View Article Online
View Journal | View Issue

Cite this: *Phys. Chem. Chem. Phys.*, 2023, **25**, 31825

Photoinduced absorption spectroscopy (PIAS) study of water and chloride oxidation by a WO_3 photoanode in acidic solution†

James Johnston, * Christopher O'Rourke and Andrew Mills

Received 5th July 2023,
Accepted 2nd November 2023

DOI: 10.1039/d3cp03167e

rsc.li/pccp

The mechanisms of water and chloride oxidation by a WO_3 photoanode are probed by photoinduced absorption spectroscopy (PIAS) coupled with transient photocurrent (TC) measurements. Linear sweep voltammograms (LSVs) and incident photon to current efficiencies (IPCEs) are obtained, in the water oxidation electrolyte (1 M $HClO_4$) and chloride oxidation electrolyte (3.5 M NaCl in 1 M $HClO_4$). Other work shows that the faradaic efficiency of water oxidation to O_2 in 1 M $HClO_4$ is *ca.* 1.0, and that for chloride oxidation to Cl_2 in 3.5 M NaCl plus 1 M $HClO_4$ is *ca.* 0.62. The PIAS/TC data reveals a 0.4 order dependency of the rate of water oxidation on the steady state concentration of photogenerated surface holes, $[h_s^+]_{ss}$, and an approximately first order dependency of the rate of chloride oxidation on $[h_s^+]_{ss}$. Associated mechanisms and rate determining steps for water and chloride oxidation at the photoanode surface that account for these reaction orders are proposed.

1. Introduction

The development of efficient solar to chemical energy conversion systems continues to be a prominent research topic in the field of semiconductor photochemistry. Most of this research has focused on an overall electrochemical process in which the reduction reaction is that of water by photogenerated electrons to produce hydrogen, and the oxidation reaction by the photogenerated holes, h^+, is either that of water (reaction (1)), *i.e.*, water-splitting,[1]

$$2H_2O + 4h^+ \rightarrow O_2 + 4H^+ \quad (1)$$

or, more recently, that of chloride, where the likely products are OCl^-/HOCl in alkaline/neutral solutions, and Cl_2 in acidic solution,[2]

$$2Cl^- + 2h^+ \rightarrow Cl_2 + 2e^- \quad (2)$$

In this work there is continuing interest in using WO_3 as a photoanode for driving reactions (1), or (2), as it is relatively inexpensive[3,4] and yet possesses a narrow band-gap of *ca.* 2.5–2.8 eV, so that its photoanode response extends into the visible region, allowing it to use *ca.* 12% of the solar spectrum.[5] However, one limitation of WO_3, is its lack of stability in alkaline solution, since above pH 5, it tends to react with OH^- to generate WO_4^{2-}, which leads to the dissolution of the photoanode.[6] Therefore, most studies of WO_3 photoanodes are conducted in acidic solution.

In any study of a photoanode for reactions (1) or (2), it is necessary to establish that the associated faradaic efficiency, f, is unity, since, depending on the electrolyte used, many other oxidation reactions are possible. For example, in 1987, Desilvestro and Grätzel, using a WO_3 photoanode in SO_4^{2-} solution, found that the faradaic efficiency for O_2 generation, f_{O_2}, decreased with decreasing pH and increasing SO_4^{2-} concentration, due to the following competing reaction,[6]

$$2SO_4^{2-} + 2h^+ \rightarrow S_2O_8^{2-} + 2e^- \quad (3)$$

More recently, Lewis *et al.* found $f_{O_2} = 0$ for a WO_3 photoanode in 1 M H_2SO_4, due to the anodic reaction (3).[7] Similarly, and possibly less surprisingly, f_{O_2} values of zero have also been reported for WO_3 photoanodes in acetic acid,[8] and methanesulfonic acid electrolytes.[9] Table 1 lists some of the major photoelectrochemical studies of WO_3 photoanodes employed to promote reactions (1) or (2) in acidic solution, in which the faradaic efficiencies of reactions (1) or (2) were reported.

The notes in Table 1 highlight the fact that in most studies conducted using a WO_3 photoanode in acidic solution with a high chloride concentration, the faradaic efficiency of chloride oxidation, f_{Cl}, has often been determined by a colourimetric method, which can assess the amount of oxidising chlorine species generated photoelectrochemically (such as Cl_2, ClO^-, HOCl, $HClO_2$, ClO_3^-), but provides no information about chemical composition and so no insight into what exactly is being generated.[11] Thus, in none of this previous work is the faradaic efficiency for Cl_2 generation, f_{Cl_2}, measured.

School of Chemistry and Chemical Engineering, Queens University Belfast, Stranmillis Road, Belfast, BT9 5AG, UK. E-mail: jjohnston497@qub.ac.uk

† Electronic supplementary information (ESI) available. See DOI: https://doi.org/10.1039/d3cp03167e

Table 1 Some studies which have reported faradaic efficiencies for water and chloride oxidation in acidic solution by WO_3 photoanodes

Annealed photoanode[a]	pH	Electrolyte anion (molarity)	f_{O_2}[b]	f_{Cl}[b]	IPCE[c]	Notes	Ref.
WO_3 powder dispersion applied to Ti sheet	1–5.5	SO_4^{2-} (0.01–3 M)	From 0.3–0.95	—	—	In SO_4^{2-} solutions, f_{O_2} increased with decreasing $[SO_4^{2-}]$ and increasing pH. Reported generation of $S_2O_8^{2-}$. f_{Cl} determined by iodometric titration.	6
	1	ClO_4^- (0.1 M)	0.81	—			
	0	Cl^- (1 M)	—	0.76			
Electro-deposited on conductive glass	0	SO_4^{2-} (1 M)	0	—	—	Proposed that ClO_4^- is oxidized to a radical, which then generates O_2 in solution.	7
	0	ClO_4^- (1 M)	*ca.* 1	—			
Aerosol assisted chemical vapour deposition	1	SO_4^{2-} (0.1 M)	0.87	—	✓	Suggested the relatively high f_{O_2} value is due to the needle nanostructure of the photoanode. Used transient diffuse reflectance spectroscopy to probe charge recombination.	10
Electro-deposition on FTO	1–6	SO_4^{2-} (0.1 M) and Cl^- (0.01–0.05 M)	—	$\leq$0.60	—	Measured free chlorine species by colourimetric method, and noted generation of ClO_3^- (by ion chromatography) under UV irradiation conditions.	11
Sol gel precursor applied by doctor blade, layer by layer	2	Cl^- (0.5 M)	—	0.70	✓	Colorimetric method was used to determine f_{Cl} (0.70). It was assumed that f_{O_2} = 0.30, but not measured.	12

[a] Photoanodes were typically annealed between 450 °C and 550 °C. [b] f_{O_2} and f_{Cl} refer here to the faradaic efficiencies of O_2 generation, and Cl^- oxidation respectively. [c] IPCE refers to the incident photon to current efficiency.

While most of the studies listed in Table 1 have reported photocurrents, and a few have included incident photon to current efficiency (IPCE) *vs.* wavelength profiles, such parameters provide little insight into the mechanism of the specific photo-oxidation reactions taking place. Recently, photoinduced absorption spectroscopy (PIAS) coupled with transient current, TC, measurements, *i.e.*, PIAS/TC, has emerged as a method for probing the mechanism of photoanodic water oxidation by relating the rate of reaction (1), as measured by the photocurrent, J, to the steady-state concentration of photogenerated surface holes, $[h_s^+]_{ss}$, as measured by the steady state absorbance change ΔAbs_{ss} of the photoanode, monitored at an appropriate wavelength.[13–16] From such measurements, the order of reaction (1) with respect to the holes, n, can be determined, thereby providing an insight into the mechanism and rate determining step. Consequently, PIAS/TC has been used to probe the mechanism of reaction (1) for a wide variety of different semiconductor oxide photoanodes, including TiO_2, Fe_2O_3, $BiVO_4$ and WO_3.[13–16] Note, however, that as the latter WO_3 PIAS/TC study was performed in H_2SO_4,[16] and f_{O_2} was not measured, it is not reasonable to assume the photo-electrochemical oxidation reaction is that of water to O_2, *i.e.*, reaction (1); indeed, for reasons outlined earlier, it is most likely that the values of n reported in this work (namely, 1 at lower surface hole densities and 2.5 at higher surface hole densities)[16] relate to either reaction (3) or a mixture of reactions (3) and (1). In contrast, in this paper, the results of a PIAS/TC mechanistic study of reactions (1) and (2), using a WO_3 photoanode in $HClO_4$ (1 M), without and with a high (3.5 M) concentration of chloride, are described, along with faradaic efficiency measurements; this combination of results is used to help identify the mechanisms associated with the major electrochemical processes associated with the observed photocurrents.

2. Experimental

2.1. Materials

Unless stated otherwise, all chemicals were purchased from Merck (Darmstadt, Germany) and used as received; the water was doubly distilled and deionised. Argon gas cylinders were purchased from BOC (Woking, UK).

2.2. Methods

2.2.1. Photoanode preparation and characterisation. The WO_3 photoanodes were prepared by a method previously reported for making P25 TiO_2 photoanodes.[17] Briefly, WO_3 nanopowder was ground repeatedly using a mortar and pestle, between additions of acetic acid (0.02 mL), water (0.1 mL), and ethanol (4.88 mL), followed by the subsequent addition of terpineol (0.43 g), and 0.74 g of an ethyl cellulose solution (10 wt% ethyl cellulose in ethanol) to create a photocatalyst paste. Paste films were then prepared by the doctor blade method, in which two strips of Scotch® Magic™ Tape were applied along parallel edges of the conductive glass substrate (fluorine-doped tin oxide (FTO), TEC 15, Pilkington Glass plc, Lancashire, UK), before *ca.* 2 mL of photocatalyst paste were applied between the tape strips, and a glass rod used to draw the paste down the length of the substrate, generating a 60 μm uniform wet film of WO_3 paste. Finally, the tape was removed, and the film was annealed at 450 °C for 30 minutes. A strip of the conductive glass substrate was kept bare in the preparation of the photoanodes, onto which adhesive copper tape was applied, to enable connection between the photoanodes and the potentiostat, *via* a crocodile clip.

2.2.2. Photoelectrochemical methods. An Autolab potentiostat (PGSTAT128 N, Metrohm, Herisau, Switzerland) was used for all electrochemical procedures. All electrochemical potentials were applied/measured with respect to a Ag/AgCl reference electrode, and thus all potential values stated herein are *vs.* a Ag/AgCl reference, unless stated otherwise. A coiled piece of Pt wire was used as the counter electrode. The electrolyte was either 1 M $HClO_4$, referred to as '$HClO_4$', for all water oxidation studies, or 3.5 M NaCl in 1 M $HClO_4$, referred to as '$NaCl/HClO_4$' for all chloride oxidation studies.

Linear sweep voltammograms, LSVs, and measurements for the faradaic efficiency of O_2 and Cl_2 generation (f_{O_2} and f_{Cl_2} respectively) were performed with the electrodes and electrolyte

housed in a PTFE electrochemical reaction cell illustrated in Section S1 in the ESI.† Prior to recording LSVs, and determining faradaic efficiencies, the electrolyte (10 mL) was purged with Ar for 10 minutes. LSVs were recorded with a scan rate of 5 mV s^{-1}. In all LSV and faradaic efficiency measurements, the photoanode was irradiated with 40 mW cm^{-2} UVA radiation, which was delivered by a 10 W, 365 nm LED (LZ4-44UV00-0000, LedEngin Inc., San Jose, US). UV irradiance was measured using a UV power meter (C10427 H10428, Hamamatsu Photonics, Hamamatsu City, Japan).

To determine f_{O_2}, an O_2 sensitive fluorescence-based sensor (O_2xyDot®, OxySense, Devens, USA) and probe (NEOFOX-GT, Ocean Insight, Orlando, USA) were used. The WO_3 photoanode was placed in the $HClO_4$ electrolyte, and while irradiated with 40 mW cm^{-2} 365 nm UVA, a potentiostat (Autolab PGSTAT128N, Metrohm AG, Herisau, Switzerland) was used to poise it at a potential (*ca.* 1.0 V *vs.* Ag/AgCl) which would generate a steady current density of 0.1 mA cm^{-2}. In this work, the reaction cell was continually flushed with Ar (0.1 mL s^{-1}), and the % O_2 in the gas outlet monitored by the O_2 sensor. The data from this study allowed the value of f_{O_2} (= *ca.* 1) to be calculated. A schematic illustration of the system, a typical set of results and their use in the subsequent calculation of f_{O_2} = *ca.* 1 are given in Section S2 of the ESI.†

To determine f_{Cl_2} for the WO_3 photoanode placed in the $NaCl/HClO_4$ electrolyte, a Drechsel bottle containing a 100 mL aqueous solution of KI (0.36 M), potassium hydrogen phthalate (0.049 M), and NaOH (0.025 M) was placed after the electrochemical cell to trap chemically from the sparging Ar stream any Cl_2 produced *via* the photoelectrochemical anodic reaction (2).[18] Thus, in this work, the WO_3 photoanode was irradiated (40 mW cm^{-2}, 365 nm) and poised at 1 V *vs.* Ag/AgCl for 30 minutes, while the sealed PTFE electrochemical reaction cell was purged continuously with Ar, thereby flushing any photogenerated Cl_2 from the reaction solution in the photoelectrochemical reactor through to the KI trap solution, where it generated I_3^-, which absorbs strongly at 353 nm (ε_{353} = 26 400 mol^{-1} cm^{-1}).[19] By measuring the absorbance of the trap solution, the concentration of I_3^-, and by extension the amount of photogenerated Cl_2, was determined. From the results of this work a f_{Cl_2} value of *ca.* 0.62 was determined for the WO_3 photoanode in the $NaCl/HClO_4$ electrolyte. A schematic illustration of the system, a typical set of results and their use in the subsequent calculation of f_{Cl_2} = *ca.* 0.62 are given in Section S3 in the ESI.† In this Cl_2-trapping experiment no O_2 was detected in the Ar purge gas stream after the trap, thereby indicating that the 0.38 deficit in the f_{Cl_2} value is due to a chloride oxidation product, which still could be Cl_2 that has reacted/decomposed before it reaches the KI trap, and/or one or more dissolved Cl^- oxidation products, such as ClO_4^-. The same Cl_2-trapping experiment carried out using a much higher irradiance (80 instead of 40 mW cm^{-2}) produced no change in f_{Cl_2}.

2.2.3. Incident photon to current efficiency, IPCE, spectra. To determine the IPCE of the WO_3 and P25 photoanodes, the samples were housed in a 3D-printed PIAS cell (illustrated in Section S4 in the ESI†), along with an Ag/AgCl reference electrode and Pt coil counter electrode. A 1 kW Xe-Arc lamp (KiloArc™, Optical Building Blocks Corporation, Pemberton, USA), coupled with a monochromator and IR filter (Optical Building Blocks Corporation, Pemberton, USA) were used to deliver radiation of known wavelength, λ_{excit}, and irradiance (units: mW cm^{-2}) to the photoanode in the PIAS cell. The wavelength range over which the value of the cell's IPCE was measured was varied from 300 to 480 nm, at 10 nm increments. At each selected value of λ_{excit}, the irradiance *vs.* wavelength profile of the excitation beam delivered to the sample was measured using a calibrated spectroradiometer (OL 756, Gooch and Housego, Ilminster, UK). At each selected value of λ_{excit}, the difference in the light on and light off current (*i.e.*, the photocurrent) was determined by chopping the incident light periodically, while poising the photoanode at 1.3 V *vs.* Ag/AgCl. Section S5 in the ESI† provides further details of this work including a schematic of the irradiation system, the irradiance *vs.* wavelength profiles of each excitation beam of value λ_{excit}, and the photocurrent response at each value of λ_{excit}, for both the water oxidation ($HClO_4$) and chloride oxidation ($NaCl/HClO_4$) systems. In addition, details of a typical calculation for the determination of the value of the IPCE at a given value of λ_{excit} are described in Section S5 in the ESI.†

2.2.4. Photoinduced absorption spectroscopy/transient photocurrent (PIAS/TC) measurements. A schematic illustration of the PIAS/TC setup is shown in Section S6 in the ESI.† In this system, a 150 W tungsten-halogen lamp, with stabilized power supply (SLS301, Thorlabs, Newton, USA), was used as the monitoring light source. The WO_3 photoanode was irradiated with a 10 W, 365 nm LED (LZ4-44UV00-0000, LedEngin Inc., San Jose, USA), the irradiance of which was varied using a variable power supply unit (QL355P, Aim and Thurlby Thandar Instruments, Huntingdon, UK) for the LED. An electronically controlled diaphragm shutter (SHB1T, Thorlabs, Newton, USA) was used to vary the duration of this UVA irradiation. Two monochromators, positioned on either side of the sample, were used to set the wavelength of the monitoring light beam that was transmitted through the WO_3 photoanode. The intensity of the transmitted light was monitored using a Si photodiode detector (DET100A2, Thorlabs, Newton, USA) coupled to an amplifier (PDA200C, ThorLabs, Newton, USA). This setup allowed the change in absorbance of the WO_3 photoanode, ΔAbs, to be determined upon its irradiation by the 365 nm LED. In this work, the WO_3 photoanode was biased at a potential of 1.3 V *vs.* Ag/AgCl, and the photocurrent monitored as a function of irradiation time at the same time as that of ΔAbs.

2.2.5. Other methods. Profilometry was performed by a Dektak^3 ST Surface Profiler (Veeco, New York, USA). UV-vis spectroscopy was performed using a Varian Cary® 50 UV-vis spectrophotometer. Diffuse reflectance measurements were performed using a hand-held spectrophotometer (KONICA MINOLTA CM-2500d, Tokyo, Japan). Powder X-ray diffraction (XRD) analysis was performed using a D8 Advance Eco diffractometer (Bruker, Massachusetts, USA) with a Cu kα X-ray source. Scanning electron microscope (SEM) images were recorded using an Environmental SEM instrument (FEI™ Quanta™ FEG 250).

3. Results and discussion

3.1. WO_3 photoanode characterisation

The thickness of the thin film of WO_3 on a typical photoanode used in this work was determined to be *ca.* 240 nm using a profilometer. The film was quite light scattering, as illustrated by the photograph in Fig. 1. As a result, the diffuse reflectance spectrum of the film was recorded, rather than its absorption spectrum, the results of which are also illustrated in Fig. 1. The results of a Tauc analysis of this spectrum (details of which are given in Section S7 in the ESI†) suggests a band gap energy, E_{bg}, of 2.7 eV, which is consistent with the value range of 2.6–2.8 eV reported previously by others for this material.[5,8,11,20]

SEM images of the surface of the WO_3 photoanode film were also recorded and the results are illustrated in Fig. 2. These images show the film comprises agglomerate particles, averaging 130 ± 30 nm in diameter, which are in turn are made up of 10 ± 2 nm diameter particles.

The XRD pattern of the WO_3 powder used to prepare the photoanodes is shown in Section S8 in the ESI† and is consistent with a monoclinic crystal structure.[22,23] The above results help define the nature the WO_3 photoanode used in this work and so aid its future reproduction by others and comparison with WO_3 photoanodes prepared using other methods, such as outlined in Table 1.

3.2. Photoelectrochemical characterisation

A detailed schematic illustration of the electrochemical cell used in this work is given in Fig. S1 in Section S1 of the ESI.† In this cell the WO_3 on FTO photoanode was used to cover the hole in the base of the photo-electrochemical reaction cell and irradiated through the back of the FTO glass. A coiled Pt wire was used as the counter electrode and an Ag/AgCl electrode was used as the reference electrode, with $HClO_4$ as the electrolyte for water oxidation and NaCl/$HClO_4$ as the electrolyte for chloride oxidation. The linear sweep voltammogram, LSV, profiles generated using this setup, both for water oxidation and chloride oxidation electrolyte, in which the applied potential was varied from −0.3 V to 2.5 V *vs.* Ag/AgCl at a sweep rate of 5 mV s^{-1}, were recorded under dark and illuminated (40 mW cm^{-2}, 365 nm) conditions. The results of this work are shown in Fig. 3, with the black and red traces corresponding to the water and chloride oxidation electrolytes, respectively. These results show that, under UV irradiation, there is an onset of photocurrent at potentials *ca.* 0.4 V, both in $HClO_4$, and NaCl/$HClO_4$ electrolytes, with the latter exhibiting a notable plateau photocurrent of *ca.* 0.62 mA cm^{-2} at *ca.* 0.8 V *vs.* Ag/AgCl, and the former reaching a much lower (by a factor of about 2) plateau photocurrent (of *ca.* 0.28 mA cm^{-2}) at *ca.* 1.35 V *vs.* Ag/AgCl.

Initially, one might expect the observed photocurrent associated with water oxidation to be larger than that for chloride, since the standard redox potential for the former is only 1.23 V, compared with 1.36 V for the latter,[7] but the larger photocurrent in the presence of Cl^- is consistent with previous reports;[3,7] for example, Lewis *et al.* reported the plateau photocurrent for their WO_3 photoanode in 1 M HCl was *ca.* 1.5×'s that in 1 M $HClO_4$.[7] The high plateau photocurrent for reaction (2), compared to that of reaction (1) is most probably due to the much simpler mechanism, and so more facile kinetics, for reaction (2), a 2 electron process, compared with reaction (1),

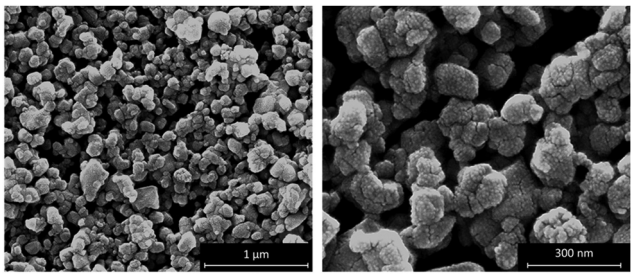

Fig. 2 SEM images of the surface of WO_3 photoanodes at 100 000× and 300 000× magnification. The average agglomerate particle size is 130 ± 30 nm agglomerates made up of 10 ± 2 nm particles.

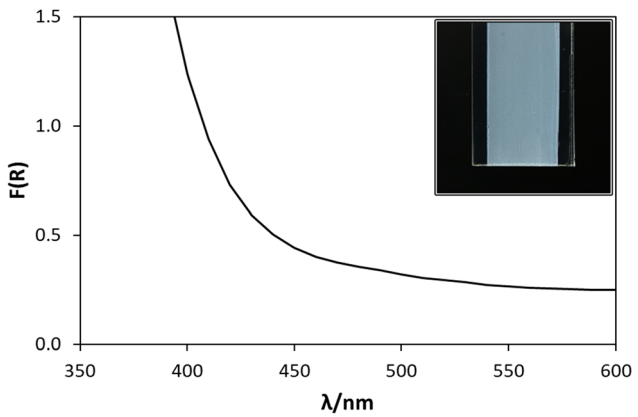

Fig. 1 $F(R)$ *vs.* λ spectrum of the WO_3 photoanode (pictured in inset image), where $F(R)$ is the Kubelka–Munk remission function, determined from the diffuse reflectance (R_λ) of the photoanode ($F(R)_\lambda = (1 - R_\lambda^2)/2R_\lambda$).[21]

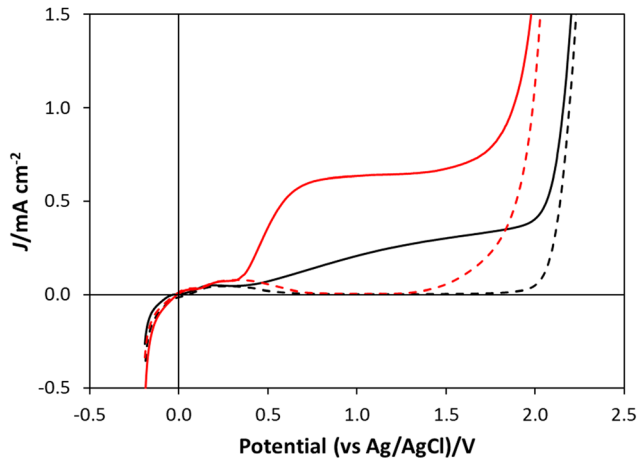

Fig. 3 Linear sweep voltammograms (LSVs) of the WO_3 photoanode in the dark (dashed traces) and under 40 mW cm^{-2}, 365 nm UVA irradiation (solid traces), in water oxidation electrolyte (1 M $HClO_4$, black traces) and chloride oxidation electrolyte (NaCl/$HClO_4$, red traces).

a 4 electron process since the more complex mechanism of the latter reaction would be expected to result in a much larger overpotential.[3] The results of stability studies on the photocurrents exhibited by the WO_3 photoanode poised at 1.3 V *vs.* Ag/AgCl in either $HClO_4$, or NaCl/$HClO_4$ solution, over 24 h irradiation are described in Section S9 in the ESI.† In both cases it appears that the photocurrents are long-lived and stable, which suggests that photocorrosion is minimal in either system.

The incident photon to current efficiency (IPCE) values were also recorded for the WO_3 photoanode in the two electrolytes (*i.e.*, $HClO_4$ or NaCl/$HClO_4$) as a function of excitation wavelength, λ_{excit}, and the results of this work are shown in Fig. 4.

From Fig. 4, the IPCE values at 365 nm in $HClO_4$ (IPCE = 2.9%) and NaCl/$HClO_4$ (IPCE = 12.9%) are both relatively low compared to IPCE values at 365 nm reported by others, such as 62% (for a 1 μm thick WO_3 photoanode in 0.1 M $HClO_4$)[24] and 71% (for a *ca.* 3 μm thick WO_3 photoanode in 0.01 M HCl/0.5 M NaCl solution).[12] However, the lower IPCE values in this work are not too surprising given that much thinner, and so more transparent, WO_3 films were used (*ca.* 240 nm thick) and so, in comparison, will absorb much less of the incident UV radiation. The much greater IPCE values recorded in NaCl/$HClO_4$, compared with $HClO_4$, are consistent with work by others,[3,7] and is most likely because (i) the overpotential for chloride oxidation, reaction (2), is significantly lower than that for water oxidation, reaction (1), and (ii) the exchange current density for reaction (2) is much greater than that for water oxidation. The IPCE spectra illustrated in Fig. 4 show that the WO_3 photoanode does indeed respond in the visible light range (between 400 nm to 450 nm), but that the photocurrent increases with decreasing λ_{excit}; a feature that is consistent with a previously reported IPCE spectrum for a WO_3 photoanode in $HClO_4$.[24]

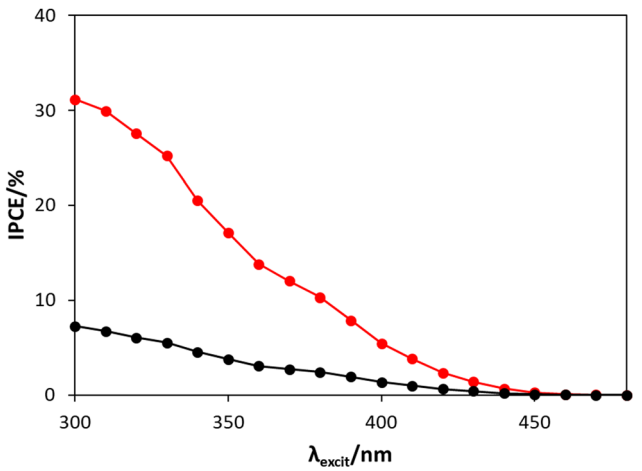

Fig. 4 The IPCE spectra between 300 to 480 nm for the WO_3 photoanode, poised at 1.3 V *vs.* Ag/AgCl, in $HClO_4$ (black) and NaCl/$HClO_4$ (red), irradiated by a combined monochromator/1 kW Xe-Arc lamp system. As noted earlier, a detailed description of how this data was obtained is given in Section S5, in the ESI.†

3.3. Photoelectrochemical water oxidation: f_{O_2}, PIAS and mechanism

As noted earlier, the faradaic efficiency of O_2 generation, f_{O_2}, using a WO_3 photoanode in $HClO_4$ was determined to be approximately unity using the method outlined in Section 2.2.2, and described in more detail in Section S2 in the ESI.† Since f_{O_2} = 1.0, this shows that reaction (1) is the photoelectrochemical reaction that occurs at the WO_3 photoanode, in 1 M $HClO_4$, when biased at *ca.* 1 V *vs.* Ag/AgCl.

The mechanism for reaction (1) was then probed using photoinduced absorbance spectroscopy (PIAS) coupled with transient photocurrent (TC) measurements. In this work, the absorbance change, ΔAbs upon UV (365 nm) irradiation of the WO_3 photoanode, poised at 1.3 V *vs.* Ag/AgCl in the water oxidation electrolyte ($HClO_4$), was monitored at 500 nm as a function of UV irradiance, ρ, as part of the PIAS study of the WO_3 photoanodes.

Note, in this work 500 nm was chosen as the monitoring light wavelength, λ_{mon}, since the transient absorbance change due to the photogeneration of long-lived, surface holes, h_s^+, on the WO_3 photoanode between 500–900 nm was found to be largest at 500 nm, see ESI,† Section S6. This observation is consistent with many, previously reported, transient absorption and diffuse reflectance studies of photogenerated holes and electrons on WO_3.[10,25,26] It is generally assumed that these holes are trapped surface holes or oxidising equivalents, h_s^+.[10,26] It is, of course, possible that in such work other trapped oxidising equivalent species (or surface holes) are photogenerated that are involved in the oxidation of water but do not contribute to the transient absorbance. Thus, it is assumed that ΔAbs provides a measure of the concentration of all such surface holes, $[h_s^+]$.

As observed in most PIAS studies of semiconductor oxide photoelectrodes, other work carried out using this system showed that ΔAbs increased with increasing polarising voltage from 0.4 to 1.8 V *vs.* Ag/AgCl, as expected if the transient absorbance was associated with photogenerated holes, and not electrons, since the greater the applied anodic bias the greater the efficiency of extracting the photo-excited electrons. In sharp contrast, work by others show that photo-excited electrons on a WO_3 photoelectrode biased at much lower potentials exhibit a ΔAbs value that increases with increasing monitoring wavelength, with a maximum *ca.* 900, not 500 nm.[25,26] Finally, note that, unless stated otherwise, all subsequent reference to holes refers to those trapped at the surface, h_s^+, rather than those generated in the bulk, h_b^+, of the semiconductor, which, as noted by others, do not make a significant contribution to the transient absorbance, 'due to their small lifetime in the bulk and the electric field drawing them to the interface with the electrolyte'.[27]

For each and every ΔAbs *vs.* time (t) plot recorded using PIAS, the corresponding photocurrent, J, *vs.* t plot was measured. Thus, in this work a series of ΔAbs *vs.* t and J *vs.* t plots were measured using the WO_3 photoanode in $HClO_4$ at different values of ρ, and the results of this work are illustrated in Fig. 5(a) and (b), respectively. Upon inspection of these figures,

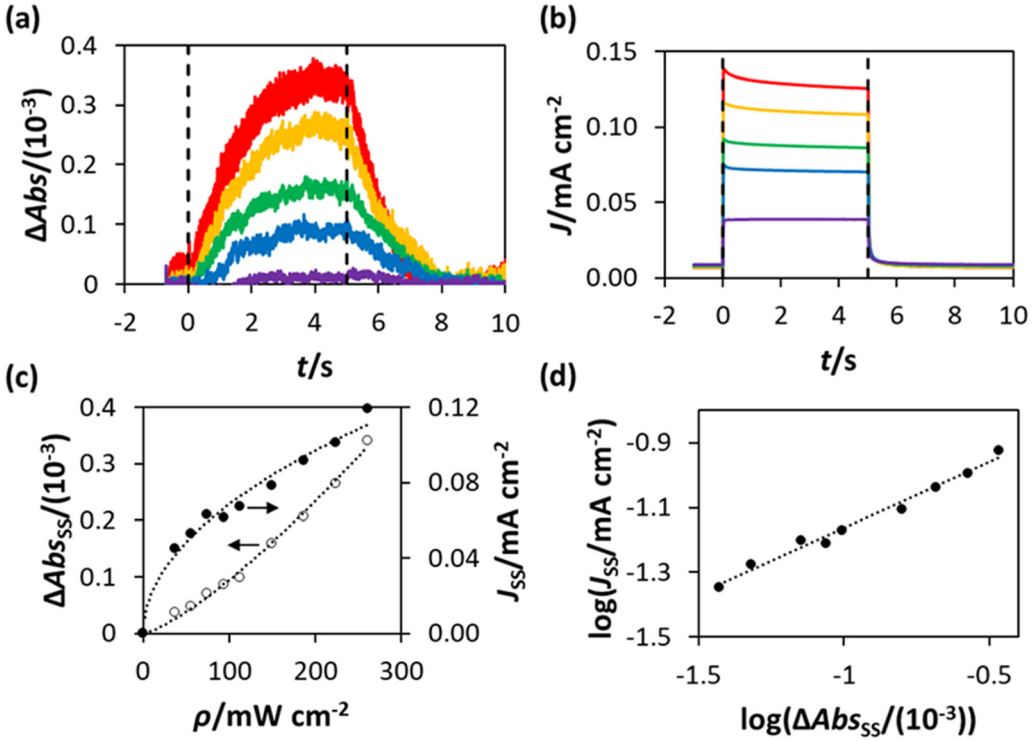

Fig. 5 PIAS/TC data obtained using the WO_3 photoanode in $HClO_4$, held at 1.3 V *vs.* Ag/AgCl, with (a) and (b) illustrating the plots of the measured value of ΔAbs and photocurrent density (J), respectively, before ($t < 0$), during ($0 < t < 5$ s) and after ($t > 5$ s) irradiation with 365 nm UVA. The irradiance (ρ) values used to obtain these traces were, from top to bottom, 260 mW cm^{-2}, 224 mW cm^{-2}, 149 mW cm^{-2}, 93 mW cm^{-2} and 19 mW cm^{-2}; (c) plots of ΔAbs_{ss} and J_{ss} *vs.* ρ, constructed from the data in (a) and (b), with lines of best fit based on $\Delta Abs_{ss} \propto \rho^{1.3}$ and $J_{ss} \propto \rho^{0.5}$, respectively; (d) plot of $\log(J_{ss})$ *vs.* $\log(\Delta Abs_{ss})$, constructed using the data in (c), yielding a straight line of best fit with a gradient = 0.4.

it is clear that the photocurrent J reaches a steady state rapidly, in less than 1 s, upon irradiation, whereas the ΔAbs response takes approximately 3 s to attain to a steady state value. Similarly, the decay in J upon the ceasing of irradiation is more rapid than the decay in ΔAbs. This is a noted, common feature of PIAS/TC studies, including those previously performed on TiO_2, hematite and $BiVO_4$ photoanodes,[13–15,28] and occurs because the electron transport to the external circuit is more rapid than the flux of photogenerated holes to the photoanode surface.[14,28]

The steady state values of the photoinduced absorbance and photocurrent were determined using the data in Fig. 5(a) and (b), *i.e.*, ΔAbs_{ss} and J_{ss}, respectively, by taking the average of the photoinduced absorbance ΔAbs and photocurrent J over the illumination period between t = 2.5 s and t = 4.5 s. The subsequent plots of ΔAbs_{ss} and J_{ss}, as a function of ρ are illustrated in Fig. 5(c), with lines of best fit showing that $\Delta Abs_{ss} \propto \rho^{1.3}$ and $J_{ss} \propto \rho^{0.5}$. It follows from the latter two expressions that $J_{ss} \propto \Delta Abs_{ss}^{0.5/1.3}$, or $\propto \Delta Abs_{ss}^{0.38}$, which is consistent with the $\log(J_{ss})$ *vs.* $\log(\Delta Abs_{ss})$ plot in Fig. 5(d), where $J_{ss} \propto \Delta Abs_{ss}^{0.4}$.

As noted earlier, since ΔAbs is assumed to be due to the photogenerated surface holes, it follows that ΔAbs_{ss} provides a direct measure of the steady state concentration of holes, $[h_s^+]_{ss}$ (by Beer's law). In this PIAS study the measured value of J_{ss} is proportional to the rate of reaction (1), R, since the f_{O_2} measurements have demonstrated that all the current is due to O_2 generation. Therefore, the rate equation for reaction (1) can be written as follows,

$$R = k[h_s^+]_{ss}^n \quad (4)$$

where, k is the rate constant, and n is the order of reaction (1) with respect to $[h_s^+]_{ss}$. It follows that eqn (4) can be rewritten, in terms of the measured parameters J_{ss} and ΔAbs_{ss}, as,

$$J_{ss} = k' \Delta Abs_{ss}^n \quad (5)$$

where k' is a constant. Thus, a plot of the data in Fig. 5(c) in the form of $\log(J_{ss})$ *vs.* $\log(\Delta Abs_{ss})$ should be a straight line of gradient n, and, as noted earlier, from such a plot, illustrated in Fig. 5(d), n = 0.4 for the photo-oxidation of water on a WO_3 photoanode in $HClO_4$.

Many different mechanisms have been proposed for the electrochemical oxidation of water on various anodes, one of which is the oxide path mechanism.[29] The latter reaction mechanism is usually given in terms of electron loss, but can be represented in terms of surface hole (h_s^+) gain, by the following reaction steps:

$$S + H_2O + h_s^+ \xrightarrow{k_6} S{-}OH + H^+ \quad (6)$$

$$2S{-}OH \xrightarrow{k_7} S{-}O + S + H_2O \quad (7)$$

$$2S{-}O \xrightarrow{k_8} S + O_2 \quad (8)$$

In this mechanism, each reaction site is either in the form of S, S–OH or S–O and so the fractions of each of these sites can be written as θ_S, θ_{SOH} and θ_{SO}, respectively, with $\theta_S + \theta_{SOH} + \theta_{SO} = 1$. If we assume the last step, reaction (8), is much faster than reactions (6) and (7), it follows that θ_{SO} is very small and so $\theta_{SOH} \approx (1 - \theta_S)$. If we also assume that under steady state reaction conditions, the rates of reactions (6) and (7) are equal, and the steady state values of θ_S and θ_{SOH} are denoted as θ_S^* and θ_{SOH}^*, then the rate of S–OH generation, $k_6\theta_S^*[H_2O][h_s^+]$, will be equal to the rate of S–OH consumption, $k_7\theta_{SOH}^{*2}$,

$$k_6\theta_S^*[H_2O][h_s^+]_{ss} = k_7(\theta_{SOH}^*)^2 \quad (9)$$

Substituting $(1 - \theta_S^*)$ for θ_{SOH}^* gives the following expression

$$k_6(\theta_S^*)[H_2O][h_s^+]_{ss} = k_7(1 - \theta_S^*)^2 \quad (10)$$

which can be rewritten as

$$\theta_S^{*2} - \theta_S^*\left(\frac{k_6[H_2O][h_s^+]_{ss}}{k_7} + 2\right) + 1 = 0 \quad (11)$$

or, replacing $k_6[H_2O][h_s^+]_{ss}/k_7$ with α,

$$\theta_S^{*2} - \theta_S^*(2 + \alpha) + 1 = 0 \quad (12)$$

Eqn (12) can be used to plot the variation of θ_S^* (and θ_{SOH}^*) with α (which is proportional to $[h_s^+]_{ss}$ and so ΔAbs_{ss}), and the resulting plot is shown in Fig. 6.

This set of model predicted data is very useful as it provides a value of θ_S^* for every value of α, which allows the calculation of a unitless form of rate of water oxidation, R', equal to R/k_7, where, from eqn (10),

$$R = k_7\alpha\theta_S^* = k_7(1 - \theta_S^*)^2 \quad (13)$$

as a function of α. The model predicted variation of R' as a function of α is illustrated in Fig. 7.

As R' is proportional to the actual rate, and therefore the steady state photocurrent, J_{ss}, *i.e.*, $J = c_1R'$, and α is proportional to $[h_s^+]_{ss}$, which in turn is proportional to ΔAbs_{ss}, or $\Delta Abs_{ss} = c_2\alpha$, it follows that through a judicious choice of values for the constants, c_1 and c_2 (0.143 and 0.0588 respectively) it should be possible to fit the observed variation in J_{ss} *vs.* ΔAbs_{ss}, to the kinetic model predicted variation in R' *vs.* α. The results of such a plot are illustrated in Fig. 8, and the excellent fit provides considerable support for the above kinetic model.

We have seen that a plot of $\log(J_{ss})$ *vs.* $\log(\Delta Abs_{ss})$ yields a straight line of gradient 0.4, implying the order of reaction, n, is 0.4. However, a brief inspection of the J_{ss} *vs.* ΔAbs_{ss} curve illustrated in Fig. 8, or its more expanded, model-generated R' *vs.* α equivalent, illustrated in Fig. 7, show that the kinetic model predicts that at low ΔAbs_{ss} values (due to a low value of ρ), J_{ss} will be proportional to ΔAbs_{ss}, *i.e.*, the reaction order with respect to ΔAbs_{ss}, n, is unity, whereas at very high ΔAbs_{ss} values (due to high ρ) J_{ss} tends to an independence of ΔAbs_{ss}, so that $n = 0$. Thus, in this work, the observation that $n = 0.4$ in the photoelectrochemical oxidation of water to O_2 by the WO_3 photoanode poised at 1.3 V *vs.* Ag/AgCl, see Fig. 5(d), is a kinetic artifact produced because the UV irradiance range used

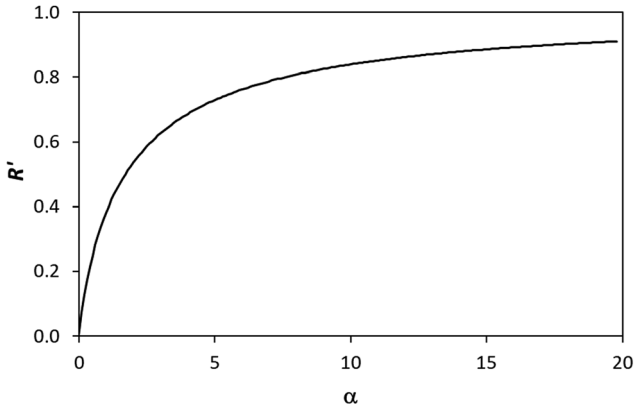

Fig. 7 Model calculated variation in R' with α, using eqn (13) and the θ_S^* and α data points in Fig. 6.

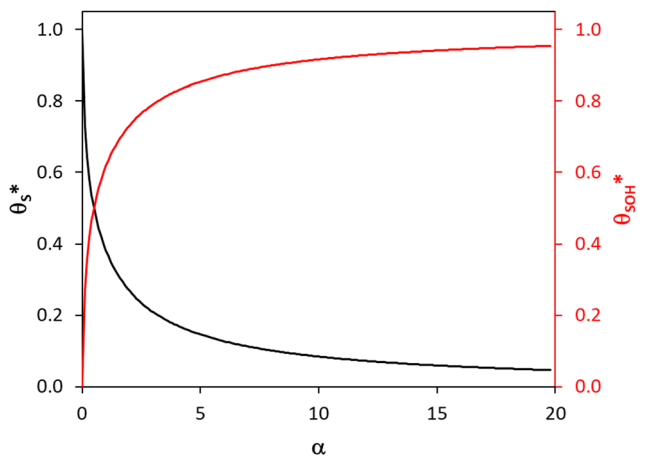

Fig. 6 The variation in θ_S^* and θ_{SOH}^* with α (in black and red respectively), as predicted by eqn (12), and the assumption that $\theta_{SOH}^* \approx 1 - \theta_S^*$.

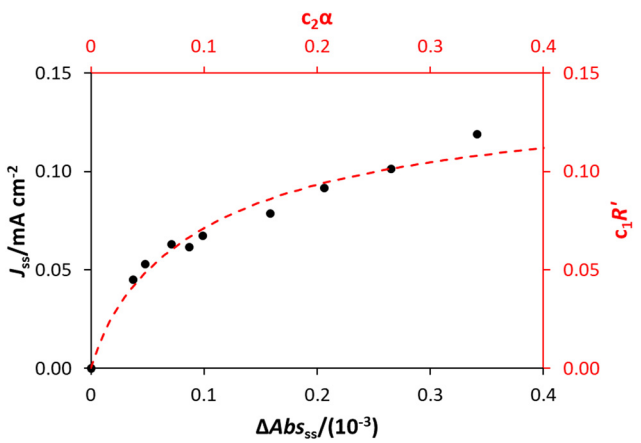

Fig. 8 The experimental values of J_{ss} and ΔAbs_{ss} are shown (in black, corresponding to the black axes), alongside the model predicted variation in R' and α according to eqn (12) and (13), multiplied by constants c_1 and c_2 (0.143 and 0.0588 respectively, shown in red).

in this work lies in between these two extremes. Support for this suggestion is provided by a log–log plot of the model predicted J_{ss} *vs.* ΔAbs_{ss} data, represented by the broken red line in Fig. 8, over the ΔAbs_{ss} range of 0.05–0.35 that is relevant to this study, which yields a good straight line with a gradient of *ca.* 0.4.

The above kinetic model also provides an insight into the dependence of the J_{ss} on the UV irradiance, ρ. In semiconductor photochemistry, the steady state concentration of the holes in the bulk, $[h_b^+]_{ss}$, is usually found to depend directly upon ρ^{ϕ}, where ϕ lies in the range 0.5 (at high ρ)–1.0 (low ρ). It appears reasonable to assume that the rate of generation of the surface (trapped) holes, h_s^+, r_g, is proportional to $[h_b^+]_{ss}$, and so $\propto \rho^{\phi}$. If the latter is the rate determining step, rds, and reactions (6) and (7) are fast, it follows that $r_6 = r_7 = r_g$, which provides a rationale for the model assumption as to why $r_6 = r_7$. In addition, given, $r_6 = r_7 = R$ (see eqn (13)), it follows,

$$R = r_g = k^{*}\rho^{\phi} \quad (14)$$

where, k^{*} is a proportionality constant. From the data in Fig. 5(c), J_{ss} (or R) is proportional to $\rho^{0.5}$, thereby indicating that in this work $\phi = 0.5$, which appears reasonable given the high UV irradiances employed (up to 250 mW cm^{-2}). Thus, the plot of J_{ss} *vs.* ρ illustrated in Fig. 5(c) is consistent with eqn (14) of the proposed kinetic model in which the rate of generation of surface holes is proportional to the steady-state concentration of holes in the bulk, $[h_b^+]_{ss}$, which in turn depends upon $\rho^{0.5}$.

By incorporating eqn (14), and the relationship $R \propto \rho^{\phi}$, into the kinetic model, it is possible to show why ΔAbs_{ss}, and so $[h_s^+]_{ss}$, is $\propto \rho^{1.3}$, as illustrated in Fig. 5(c). Thus, assuming $\phi = 0.5$, the combination of eqn (13) and (14) yields the following expression relating the UV irradiance, ρ, to the product of α (which is proportional to ΔAbs_{ss}) and θ_S^*,

$$\rho = \left(k_7 \alpha \theta_S^* / k^*\right)^2 = c_3 \left(\alpha \theta_S^*\right)^2 \quad (15)$$

where c_3 is a proportionality constant. Thus, the kinetic model equivalent of the plot of ΔAbs_{ss} *vs.* ρ, as illustrated in Fig. 5(c), is a plot of α *vs.* $\left(\alpha\theta_S^*\right)^2$, Fig. 9, generated using the model-calculated values of α and θ_S^* (illustrated in Fig. 6).

The results of such a plot are illustrated in Fig. 9 (main diagram) and show that the kinetic model predicted variation of α *vs.* $\left(\alpha\theta_S^*\right)^2$, has a similar, non-linear shape to that of the plot of ΔAbs_{ss} *vs.* ρ illustrated in Fig. 5(c). To test this similarity further, the model-generated results illustrated in Fig. 9 were then fitted to the ΔAbs_{ss} *vs.* ρ data points in Fig. 5(c), as illustrated in the insert diagram in Fig. 9, using values for the proportionality constants, c_2 and c_3 of 0.0588 and 445, respectively. The excellent fit of the kinetic model predicted variation in ΔAbs_{ss} *vs.* ρ (broken red line) to the measured ΔAbs_{ss} *vs.* ρ data points, as illustrated in the insert plot in Fig. 9 provides further support for the proposed kinetic model. A log–log plot of the kinetic model predicted ΔAbs_{ss} *vs.* ρ data used to generate the broken red line in the latter plot yields a straight line with a gradient of 1.3, in agreement with the finding that $\Delta Abs_{ss} \propto \rho^{1.3}$, as noted earlier for the data points in Fig. 5(c).

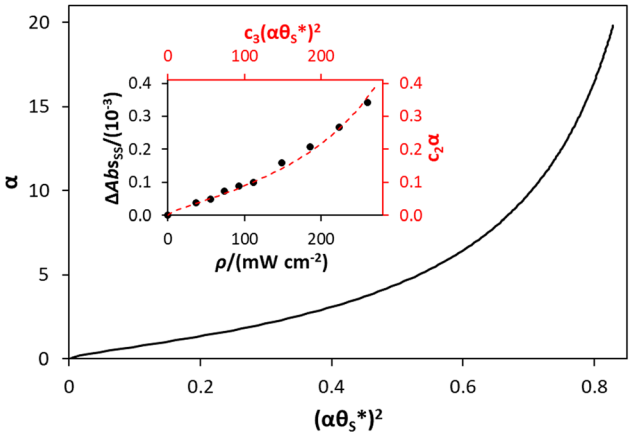

Fig. 9 Plot of α *vs.* $\left(\alpha\theta_S^*\right)^2$ (model equivalent to ΔAbs_{ss} *vs.* ρ) using the model-calculated values of α and θ_S^* shown in Fig. 6. The insert diagram is the plot of ΔAbs_{ss} *vs.* ρ data points shown in Fig. 5(c), along with a plot of the appropriate model data in the main diagram in the form of $c_2\alpha$ *vs.* $c_3\left(\alpha\theta_S^*\right)^2$, where c_2 and c_3 are equal to 0.0588 and 445, respectively.

Alternatively, assuming reaction (7) is the rds, the unreacted sites S would be depleted as ρ is increased, since $\theta_{SOH}^* = \left(1 - \theta_S^*\right)$ and hence the surface hole population will increase to maintain $r_6 = r_7$. Thus, as ρ is increased, the concentration of holes accumulated increases, thereby pushing up the ΔAbs_{ss} *vs.* ρ curve to be proportional to $\rho^{1.3}$.

In summary, in the system under study, it appears that $[h_b^+]_{ss}$ is proportional to $\rho^{0.5}$, so that the overall rate, J_{ss} (or R) is $\propto \rho^{0.5}$ and that ΔAbs_{ss} (and so $[h_s^+]_{ss}$ and α) is proportional to $\rho^{1.3}$. The latter feature is due to the non-linear decrease in the fraction of reaction sites, θ_S^*, with increasing α (or ΔAbs_{ss}), see Fig. 6. Thus, with increasing ρ, θ_S^* is eventually reduced to such an extent that an increasing concentration of photogenerated surface holes is required in order to produce the same incremental increase in rate. This increasing accumulation of surface holes with increasing ρ is responsible for the observation that ΔAbs_{ss} (and so $[h_s^+]_{ss}$) is $\propto \rho^{1.3}$.

3.3.1. Photoelectrochemical chloride oxidation. As noted earlier, for the WO_3 photoanode in NaCl/$HClO_4$, irradiated with UVA (40 mW cm^{-2} 365 nm) whilst poised at 1 V *vs.* Ag/AgCl, the value of f_{Cl_2} was determined to be 0.62. Thus, although the major anodic reaction at the WO_3 photoanode, is reaction (2), 38% of the charge transferred appears to be associated with another oxidation reaction. The most obvious competing reaction is the oxidation of water, however, as noted earlier, no O_2 was detected in the Ar gas stream after the KI trap and other work showed that no ClO_3^- was produced by this system (see Section S10 in the ESI†). One possible explanation for the unaccounted for 38% of the charge could be that it is associated with the oxidation of Cl^- to perchlorate, ClO_4^-, as is known to occur on Fe_3O_4 anodes under acidic conditions.[30] Another possibility is that the value of f_{Cl_2} was actually near to unity, but that a significant fraction of the Cl_2 was removed, by reacting with parts of the cell and tubing, before it reached the KI trap. As a consequence, although the major oxidation product is Cl_2, any mechanistic interpretation of the results

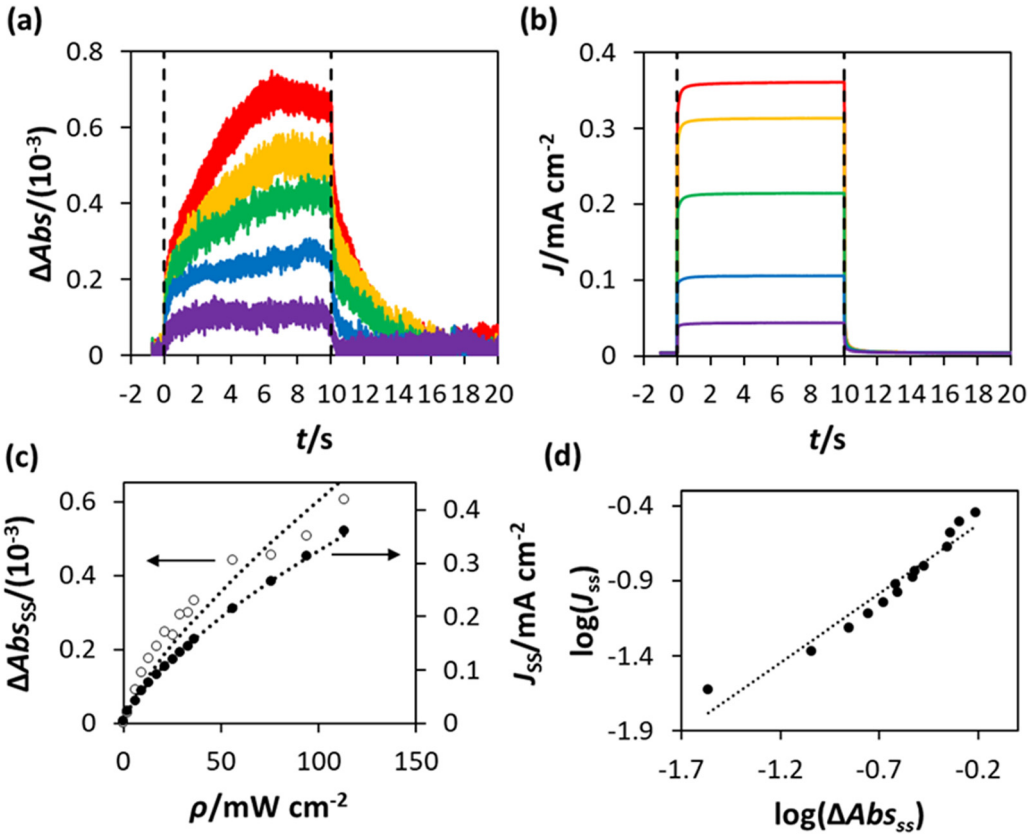

Fig. 10 PIAS/TC data obtained using the WO_3 photoanode in NaCl/$HClO_4$, held at 1.3 V *vs.* Ag/AgCl, with (a) and (b) illustrating the plots of the measured value of ΔAbs and photocurrent density (*J*), respectively, before ($t < 0$), during ($0 < t < 10$ s) and after ($t > 10$ s) irradiation with 365 nm UVA. The irradiance (ρ) values used to obtain these traces were, from top to bottom, 113 mW cm^{-2}, 94 mW cm^{-2}, 56 mW cm^{-2}, 21 mW cm^{-2} and 6 mW cm^{-2}; (c) plots of ΔAbs_{ss} and J_{ss} *vs.* ρ, constructed from the data in (a) and (b), with lines of best fit based on $\Delta Abs_{ss} \propto \rho^{0.75}$ and $J_{ss} \propto \rho^{0.7}$; (d) plot of $\log(J_{ss})$ *vs.* $\log(\Delta Abs_{ss})$, constructed using the data in (c), yielding a straight line of best fit with a gradient = 0.9.

generated in a subsequent study of the system using PIAS/TC is limited.

PIAS/TC data was obtained for the WO_3 photoanode, poised at 1.3 V (*vs.* Ag/AgCl), in the chloride oxidation electrolyte (NaCl/$HClO_4$) using the same procedures used when the electrolyte was $HClO_4$. The resulting plots of ΔAbs (λ_{mon} = 500 nm) and *J vs. t*, are shown in Fig. 10(a) and (b) respectively. The plateau, steady-state values of ΔAbs and *J* upon irradiation (ΔAbs_{ss} and J_{ss}) were then calculated as the average values between t = 6 s and t = 9.5 s, and the results plotted as a function of the irradiance used to obtain them, ρ, in Fig. 10(c) with lines of best fit based on $\Delta Abs_{ss} \propto \rho^{0.75}$ and $J_{ss} \propto \rho^{0.7}$, so that $J_{ss} \propto \Delta Abs_{ss}^{0.9}$, as also revealed by Fig. 10(d). A plot of the data in Fig. 10(c) in the form of $\log(J_{ss})$ *vs.* $\log(\Delta Abs_{ss})$, Fig. 10(d), produced a straight line with a gradient = 0.9, suggesting that the order of reaction, n_{Cl}, for the oxidation of chloride by the photogenerated surface holes is ≈ 1.

As noted above, although f_{Cl_2} = 0.62, no O_2 evolution was observed, and so the unaccounted 0.38 in faradaic efficiency is most likely due to a chloride oxidation product, such as ClO_4^-, or even pre-trap Cl_2 lost due to its high reactivity. As a consequence, it would seem reasonable to assume that whatever the chloride photoelectrochemical product, the rds is the same. If, as before, we assume that the rate of generation of the surface (trapped) holes, h_s^+, r_g, is proportional to $[h_b^+]_{ss}$, and so proportional to ρ^{ϕ}, and the latter is the rds, then eqn (14) will apply and, since the results in Fig. 10(c) reveal J_{ss} (or *R*) is proportional to $\rho^{0.7}$, it follows that in the photo-oxidation of chloride, ϕ = 0.7. The latter value for the photo-oxidation of chloride, compared with 0.5 for water oxidation, appears reasonable given the much lower high UV irradiances employed (<120 mW cm^{-2}). Many proposed mechanisms for chloride oxidation in acidic solution on metal oxide anodes have the same first step, the oxidation of a Cl^- ion,[31,32]

$$S + Cl^- + h_s^+ \rightarrow S\text{–}Cl \quad (16)$$

If we assume this, and all subsequent steps are facile, so that $\alpha\theta_S^*$ is ≈ 1, then, the rate of generation of surface holes, r_g, $\propto \rho^{0.7}$, would be proportional to the rate of their loss, $k_{16}[h_s^+]_{ss}$, and since $[h_s^+]_{ss}$ is proportional to ΔAbs_{ss} it follows that ΔAbs_{ss} will be proportional to $\rho^{0.7}$. This prediction appears roughly consistent with the finding that ΔAbs_{ss} is proportional to $\rho^{0.75}$, as illustrated by the data in Fig. 10(c). In addition, a PIAS/TC study of such a system would be expected to yield a set of J_{ss} and ΔAbs_{ss}, recorded at different values of ρ, which when plotted in

the form of $\log(J_{ss})$ *vs.* $\log(\Delta Abs_{ss})$ would produce a straight line with a gradient of unity. The measured variation in $\log(J_{ss})$ *vs.* $\log(\Delta Abs_{ss})$, with gradient = 0.9 not 1.0, see Fig. 10(d), appears approximately consistent with this kinetic model prediction, and suggests that whatever the final chloride oxidation product, be it all Cl_2 or 62% Cl_2 and the rest ClO_4^-, reaction (16) is likely a common initial step.

4. Conclusion

PIAS/TC was used to identify for a WO_3 photoanode the dependency of the rate determining steps of both water and chloride oxidation on photogenerated surface holes, h_s^+. Water oxidation, in $HClO_4$, proceeds with unity faradaic efficiency, and with a rate proportional to $[h_s^+]_{ss}^{0.4}$. This order is best understood as being between the two extremes of first order and zero order, indicating that at lower irradiations, the rate tends towards a first order dependence on $[h_s^+]_{ss}$, but at higher irradiances, the photoanode surface becomes saturated with OH and O groups, and the rate tends towards independence of $[h_s^+]_{ss}$. The PIAS/TC study of WO_3 chloride oxidation, on the other hand, revealed an approximately first order dependence of the rate on $[h_s^+]_{ss}$, despite a faradaic efficiency for Cl_2 production of 0.62, which possibly suggests a mixture of Cl_2 and ClO_4^- is produced. However, the approximate first order relationship between rate and $[h_s^+]_{ss}$ observed in the acidic chloride solution indicates that the reaction mechanisms generating both Cl_2, and possibly some other chloride oxidation product, have the same initial step, which most likely involves the photoelectrochemical oxidation of an adsorbed Cl^- ion. The results of this work provide previously unavailable insights into the mechanism of water and chloride oxidation in acidic solution that occur on a WO_3 photoanode which may prove useful in the eventual development of efficient water/saltwater splitting photoelectrochemical systems.

Data access

All data is provided in full in the results section of this paper and ESI† accompanying this paper.

Author contributions

James Johnston: investigation, visualization, writing (original draft); Christopher O'Rourke: investigation, methodology, visualization; Andrew Mills: conceptualization, supervision, writing (review and editing).

Conflicts of interest

There are no conflicts to declare.

Acknowledgements

We are grateful for support from the Catalysis Hub funded by EPSRC grant reference EP/R026645/1.

References

1 C. Jiang, S. J. A. Moniz, A. Wang, T. Zhang and J. Tang, *Chem. Soc. Rev.*, 2017, **46**, 4645–4660.
2 C. R. Lhermitte and K. Sivula, *ACS Catal.*, 2019, **9**, 2007–2017.
3 J. Juodkazytė, M. Petrulevičienė, M. Parvin, B. Šebeka, I. Savickaja, V. Pakštas, A. Naujokaitis, J. Virkutis and A. Gegeckas, *J. Electroanal. Chem.*, 2020, **871**, 114277.
4 S. Ahmed, I. A. Hassan, H. Roy and F. Marken, *J. Phys. Chem. C*, 2013, **117**, 7005–7012.
5 S. S. Kalanur, L. T. Duy and H. Seo, *Top. Catal.*, 2018, **61**, 1043–1076.
6 J. Desilvestro and M. Grätzel, *J. Electroanal. Chem. Interfacial Electrochem.*, 1987, **238**, 129–150.
7 Q. Mi, A. Zhanaidarova, B. S. Brunschwig, H. B. Gray and N. S. Lewis, *Energy Environ. Sci.*, 2012, **5**, 5694–5700.
8 J. C. Hill and K.-S. Choi, *J. Phys. Chem. C*, 2012, **116**, 7612–7620.
9 S. Reinhard, F. Rechberger and M. Niederberger, *ChemPlusChem*, 2016, **81**, 935–940.
10 S. Corby, L. Francàs, S. Selim, M. Sachs, C. Blackman, A. Kafizas and J. R. Durrant, *J. Am. Chem. Soc.*, 2018, **140**, 16168–16177.
11 M. S. Koo, X. Chen, K. Cho, T. An and W. Choi, *Environ. Sci. Technol.*, 2019, **53**, 9926–9936.
12 M. Jadwiszczak, K. Jakubow-Piotrowska, P. Kedzierzawski, K. Bienkowski and J. Augustynski, *Adv. Energy Mater.*, 2020, **10**, 1903213.
13 A. Kafizas, Y. Ma, E. Pastor, S. R. Pendlebury, C. Mesa, L. Francàs, F. Le Formal, N. Noor, M. Ling and C. Sotelo-Vazquez, *ACS Catal.*, 2017, **7**, 4896–4903.
14 F. Le Formal, E. Pastor, S. D. Tilley, C. A. Mesa, S. R. Pendlebury, M. Grätzel and J. R. Durrant, *J. Am. Chem. Soc.*, 2015, **137**, 6629–6637.
15 Y. Ma, C. A. Mesa, E. Pastor, A. Kafizas, L. Francàs, F. Le Formal, S. R. Pendlebury and J. R. Durrant, *ACS Energy Lett.*, 2016, **1**, 618–623.
16 C. A. Mesa, L. Francas, K. R. Yang, P. Garrido-Barros, E. Pastor, Y. Ma, A. Kafizas, T. E. Rosser, M. T. Mayer and E. Reisner, *Nat. Chem.*, 2020, **12**, 82–89.
17 C. O'Rourke and A. Mills, *Chem. Commun.*, 2021, **57**, 1242–1245.
18 A. Mills and A. Cook, *Analyst*, 1987, **112**, 1289–1291.
19 A. D. Awtrey and R. E. Connick, *J. Am. Chem. Soc.*, 1951, **73**, 1842–1843.
20 M. Butler, *J. Appl. Phys.*, 1977, **48**, 1914–1920.
21 K. D. Dahm and D. J. Dahm, in *Handbook of Near-Infrared Analysis*, ed. E. W. Ciurczak, B. Igne, J. Workman and D. A. Burns, CRC Press, Boca Raton, 4th edn, 2021, ch. 3, p. 33.
22 ICDD, International Centre for Diffraction Data (ICDD), **https://www.icdd.com/**, (accessed October 2023).
23 COD, Crystallography Open Database 1528915, **https://qiserver.ugr.es/cod/1528915.html**, (accessed October 2023).
24 N. Gaikwad, G. Waldner, A. Brüger, A. Belaidi, S. Chaqour and M. Neumann-Spallart, *J. Electrochem. Soc.*, 2005, **152**, G411.
25 F. M. Pesci, A. J. Cowan, B. D. Alexander, J. R. Durrant and D. R. Klug, *J. Phys. Chem. Lett.*, 2011, **2**, 1900–1903.
26 S. Corby, E. Pastor, Y. Dong, X. Zheng, L. Francàs, M. Sachs, S. Selim, A. Kafizas, A. A. Bakulin and J. R. Durrant, *J. Phys. Chem. Lett.*, 2019, **10**, 5395–5401.

27 L. Francàs, C. A. Mesa, E. Pastor, F. Le Formal and J. R. Durrant, in *Advances in Photoelectrochemical Water splitting*, ed. S. D. Tilley, S. Lany and R. van de Krol, RSC, Cambridge, 2018, ch. 5, p. 132.
28 C. A. Mesa, A. Kafizas, L. Francàs, S. R. Pendlebury, E. Pastor, Y. Ma, F. Le Formal, M. T. Mayer, M. Grätzel and J. R. Durrant, *J. Am. Chem. Soc.*, 2017, **139**, 11537–11543.
29 J. O. M. Bockris, *J. Chem. Phys.*, 1956, **24**, 817–827.
30 E. C. Walker, *Method of electrolytic production of perchloric acid*, *US. Pat.*, US1271633A, **https://patents.google.com/patent/US1271633A/en**, 2023.
31 S. Trasatti, *Electrodes of Conductive Metallic Oxides: Part B*, Elsevier Science Ltd, 1981.
32 S. Trasatti, *Electrochim. Acta*, 1987, **32**, 369–382.